arXiv:1002.3155v1 [cond-mat.mes-hall] 16 Feb 2010

Wormhole Effect in a Strong Topological Insulator

G. Rosenberg, H.-M. Guo and M. Franz
Department of Physics and Astronomy, University of British Columbia, Vancouver, BC, Canada V6T 1Z1

(Dated: February 16, 2010)

An infinitely thin solenoid carrying magnetic flux Φ (a 'Dirac string') inserted into an ordinary band insulator has no significant effect on the spectrum of electrons. In a strong topological insulator, remarkably, such a solenoid carries protected gapless one-dimensional fermionic modes when $\Phi = hc/2e$. These modes are spin-filtered and represent a distinct bulk manifestation of the topologically non-trivial insulator. We establish this 'wormhole' effect by both general qualitative considerations and by numerical calculations within a minimal lattice model. We also discuss the possibility of experimental observation of a closely related effect in artificially engineered nanostructures.

PACS numbers: 73.43.-f, 72.80.Sk, 73.20.-r

Surface electrons in a strong topological insulator (STI) [1–8] form a gapless helical liquid, protected by time reversal symmetry ($\mathcal{T}$) through the topological invariants that characterize the bulk band structure. When $\mathcal{T}$ is broken, which may be accomplished by coating the surface with a ferromagnetic film, the helical liquid transforms into an exotic insulating state characterized by a precisely quantized Hall conductivity

$$\sigma_{xy} = \left(n + \frac{1}{2}\right)\frac{e^2}{h}, \tag{1}$$

with n integer. This result follows from the microscopic theory of the surface state [3] and also from the effective electromagnetic action describing the bulk of a topological insulator, which contains the axion term [9, 10]. Although it might not be possible to measure this 'fractional' quantum Hall effect in a transport experiment [11], Eq. (1) is predicted to have observable physical consequences, such as the low-frequency Faraday rotation [9] and the image magnetic monopole effect [12].

It is instructive to apply Laughlin's flux insertion argument [13] to the STI surface described by Eq. (1). This argument was devised to establish the fractional charge of quasiparticles in fractional quantum Hall liquids (FQHL) [14] and involves the adiabatic insertion of an infinitely thin solenoid carrying magnetic flux $\Phi(t)$ into the system, as illustrated in Fig. 1a. As the flux is ramped up from 0 to $\Phi_0 = hc/e$, a circumferential electric field is generated in accord with Faraday's law $\nabla \times \mathbf{E} = -(1/c)(\partial \mathbf{B}/\partial t)$. This induces a Hall current on the STI surface $\mathbf{j} = \sigma_{xy}(\mathbf{E} \times \hat{z})$ which brings electric charge

$$\delta Q = \sigma_{xy}\frac{\Phi_0}{c} = \left(n + \frac{1}{2}\right)e \tag{2}$$

to the solenoid. Since the flux tube carrying a full flux quantum Φ_0 can be removed from the electronic Hamiltonian by a gauge transformation, one concludes, as in FQHL, that an excitation with fractional charge (2) must exist. This finding stands in contradiction to the well established microscopic theory of these surface states given by an odd number of massive Dirac Hamiltonians [3]. Elementary excitations of a massive Dirac Hamiltonian are particle-hole pairs which are charge neutral. Yet, this same Dirac Hamiltonian exhibits Hall conductivity (1), which, through Laughlin's argument outlined above, implies fractionally charged quasiparticles.

The resolution to this paradox comes from the realization that the quantum Hall state realized on the surface of a STI is inextricably linked to the bulk of the STI. Laughlin's argument fails because the flux tube inserted into the *bulk* of the STI is not inert. We demonstrate below that when $\Phi = (s + 1/2)\Phi_0$, with s integer, the flux tube carries topologically protected gapless fermionic modes and forms a conducting quantum wire – a 'wormhole' – along which the accumulated surface charge can escape to another surface of the sample. In the end, no net fractional charge is accumulated at the surface and Laughlin's argument instead predicts, indirectly, a new effect associated with a Dirac string in the bulk of a STI that we propose to call a 'wormhole effect'.

In the rest of this Letter we establish the wormhole effect, first by an analytical calculation using the universal properties of the surface states, and then by numerical calculations within a lattice model of a STI. We discuss

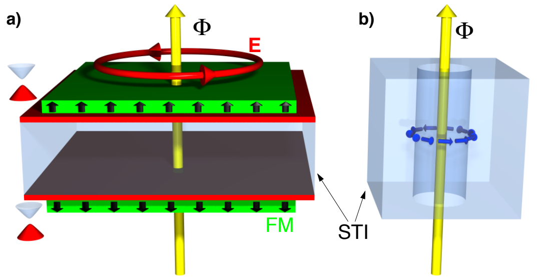

FIG. 1: (Color online) a) Topological insulator coated with a ferromagnetic (FM) film. The flux tube employed in Laughlin's argument and the induced electric field are indicated. b) Flux tube threading a cylindrical hole in a STI. Arrows illustrate the helical spin state for upward moving electrons (for down-movers the arrows are reversed).

its physical properties, significance and the possibility of experimental observation.

We begin by considering a bulk STI with a cylindrical hole of radius R threaded by magnetic flux $\Phi = \eta\Phi_0$ with $0 \le \eta < 1$ as illustrated in Fig. 1b. By solving the Dirac equation for the surface electrons we show that a gapless state exists when $\eta = \frac{1}{2}$ and persists in the limit $R \to 0$. According to Ref. [15] electron states on a curved surface of a STI, characterized by a normal unit vector $\hat{\mathbf{n}}$, are described by a Dirac Hamiltonian of the form

$$\mathcal{H} = \frac{1}{2}v\big[\hbar\nabla\cdot\hat{\mathbf{n}} + \hat{\mathbf{n}}\cdot(\mathbf{p}\times\boldsymbol{\sigma}) + (\mathbf{p}\times\boldsymbol{\sigma})\cdot\hat{\mathbf{n}}\big] \tag{3}$$

where v is the Dirac velocity, $\mathbf{p} = -i\hbar\nabla$ is the momentum operator and $\boldsymbol{\sigma} = (\sigma_1, \sigma_2, \sigma_3)$ is the vector of Pauli spin matrices. The magnetic flux is included by replacing $\mathbf{p}$ with $\boldsymbol{\pi} = \mathbf{p} - (e/c)\mathbf{A}$, where $\mathbf{A} = \eta\Phi_0(\hat{z}\times\mathbf{r})/2\pi r^2$ is the vector potential. For a cylindrical inner surface $\hat{\mathbf{n}} = -(\cos\varphi, \sin\varphi, 0)$, the Hamiltonian (3) becomes, in cylindrical coordinates and taking $v = \hbar = 1$,

$$\mathcal{H}_k = -\frac{1}{2R} + \begin{pmatrix} \frac{1}{R}(i\partial_\varphi + \eta) & -ike^{-i\varphi} \\ ike^{i\varphi} & -\frac{1}{R}(i\partial_\varphi + \eta) \end{pmatrix}. \tag{4}$$

We assumed a plane-wave solution e^{ikz} along the cylinder axis and replaced $-i\partial_z \to k$.

The eigenstates of $\mathcal{H}_k$ are of the form

$$\Psi_k(\varphi) = \begin{pmatrix} f_k \\ e^{i\varphi}g_k \end{pmatrix} e^{i\varphi l} \tag{5}$$

with l integer. The spinor $\tilde{\Psi}_k = (f_k, g_k)^T$ is an eigenstate of $\tilde{\mathcal{H}}_{kl} = \sigma_2 k - \sigma_3(l + \frac{1}{2} - \eta)/R$ with an energy eigenvalue

$$E_{kl} = \pm v\hbar\sqrt{k^2 + \frac{(l + \frac{1}{2} - \eta)^2}{R^2}}. \tag{6}$$

For a generic strength of the magnetic flux the spectrum of electrons along the cylindrical surface shows a gap

$$\Delta = \frac{2v\hbar}{R}\left|\frac{1}{2} - \eta\right|. \tag{7}$$

When $\eta = \frac{1}{2}$, *i.e.* at half flux quantum, the $l = 0$ mode becomes gapless, $E_{k0}^{\eta=1/2} = \pm v\hbar|k|$, independent of the hole radius R. This is the wormhole effect introduced above. Physically, the necessity of the flux for the gapless state to occur stems from the Berry's phase π acquired by electron spins in the helical state depicted in Fig. 1b. The gapless state occurs at half flux quantum when the Aharonov-Bohm phase exactly cancels the spin Berry's phase.

We observe that the system remains $\mathcal{T}$-invariant in the presence of a half flux quantum threading the hole. Therefore, the gapless state is topologically protected against any weak perturbation that respects $\mathcal{T}$ and does not close the bulk gap. Specifically, it should be robust against weak non-magnetic disorder as well as any smooth deformation of the hole. Our numerical simulations, presented below, provide support for this topological protection.

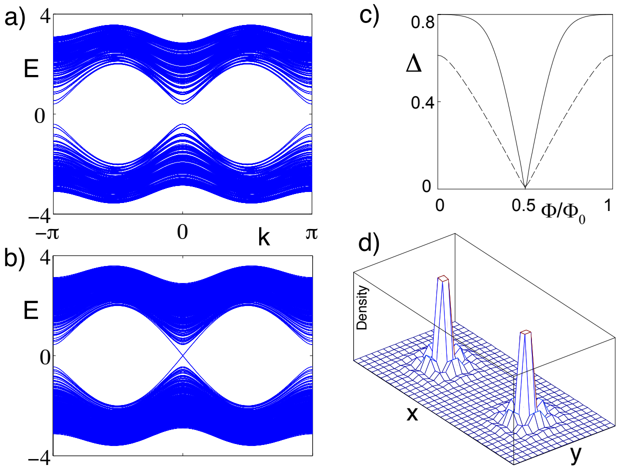

FIG. 2: (Color online) Band structure of 36×18 STI sample (periodic boundary conditions), infinite along the z-direction with two flux tubes carrying flux $\eta\Phi_0$ and $-\eta\Phi_0$ inserted, a) $\eta = 0$, b) $\eta = 1/2$. Panel c) shows dependence of the spectral gap on the flux for thin flux tubes threading a lattice plaquette (solid line), and thicker flux tube threading a 3×3 rectangular hole (dashed line). d) Wavefunction amplitude for a low-lying state extended along the flux tubes. Parameters used here are $t = 0.2$, $\epsilon = 0.8$.

We now study the wormhole effect using a concrete lattice model of a topological insulator which we solve by exact numerical diagonalization. In order to keep the computational difficulties at a minimum we consider a simple model on a cubic lattice discussed previously [9, 16]. This minimal model has two electron orbitals per lattice site, denoted c and d, and is defined by the momentum space Hamiltonian $H = \sum_{\mathbf{k}} \Psi_{\mathbf{k}}^\dagger \mathcal{H}_{\mathbf{k}} \Psi_{\mathbf{k}}$ with $\Psi_{\mathbf{k}} = (c_{\mathbf{k}\uparrow}, c_{\mathbf{k}\downarrow}, d_{\mathbf{k}\uparrow}, d_{\mathbf{k}\downarrow})^T$,

$$\mathcal{H}_{\mathbf{k}} = -2\lambda\sum_\mu \tau_z\sigma_\mu \sin k_\mu + \tau_x m_{\mathbf{k}}, \tag{8}$$

and $m_{\mathbf{k}} = \epsilon - 2t\sum_\mu \cos k_\mu$. Here τ_μ and σ_μ are Pauli matrices in orbital and spin space, respectively, with $\mu = x, y, z$. The system defined by H is invariant under time-reversal and spatial inversion. The spectrum of excitations has two doubly degenerate bands,

$$E_{\mathbf{k}} = \pm\sqrt{4\lambda^2(\sin^2 k_x + \sin^2 k_y + \sin^2 k_z) + m_{\mathbf{k}}^2}. \tag{9}$$

At half filling, depending on the values of the parameters λ, t, ϵ, the system can be a trivial insulator, as well as a strong and weak topological insulator (WTI) [9, 16]. Below, unless stated otherwise, we work with parameters

$2t < \epsilon < 6t$, corresponding to a STI phase characterized by the Z_2 invariant $(1;000)$. All energies are expressed in units of λ which we take equal to 1.

To look for gapless propagating modes along a flux tube we first consider a sample infinite in the z-direction with a rectangular base containing $2L \times L$ sites. Two straight flux tubes carrying fluxes $\eta\Phi_0$ and $-\eta\Phi_0$ along the z-direction are positioned a distance L apart on the x axis. Since the total flux threading the system is zero for this arrangement we may use periodic boundary conditions along x and y and thus eliminate gapless modes that would otherwise reside on surfaces. Results for $L = 18$ are displayed in Fig. 2. Without the flux ($\eta = 0$) the system shows a spectral gap. For $\eta > 0$ subgap states appear near $k = 0$. When $\eta = \frac{1}{2}$ a gapless mode exists along each of the flux tubes.

In addition to thin flux tubes that thread an elementary plaquette we also considered flux threading a larger rectangular hole in the sample. Results for this case are similar; a gapless mode appears when $\eta = \frac{1}{2}$ and the dependence of the gap on η (Fig. 2c) now more closely resembles that given in Eq. (7). In general gapless modes persist for any size and shape of the hole, as long as it is threaded by a half flux quantum.

We performed similar calculations for other topological phases occurring in the same model. In a $(1;111)$ STI that occurs when $-6t < \epsilon < -2t$ a single gapless mode (per flux tube) exists, now located near $k = \pi$. In WTI phases an even number of gapless modes per flux tube appear. For a straight flux tube along direction $\hat{\mathbf{n}}$ we find two gapless modes (one at $k = 0$ and one at $k = \pi$) when $\hat{\mathbf{n}} \cdot \boldsymbol{\nu} \neq 0$ and zero otherwise. Here $\boldsymbol{\nu} = (\nu_1\nu_2\nu_3)$. Finally, we have verified that in a trivial $(0;000)$ insulator, that occurs for $|\epsilon| > 6t$, no gapless modes appear for any direction or strength of flux tube.

Using our model with a single flux tube in a geometry with open boundary conditions it is possible to visualize the flow of charge at the intermediate steps of Laughlin's flux insertion argument. To this end we consider a cube of size L^3 and supplement the Hamiltonian (8) with a surface magnetization term

$$H_S = -\Omega_S \sum_{j\in \mathrm{surf}} \hat{\mathbf{r}}_j \cdot \left(\Psi_j^\dagger \boldsymbol{\sigma} \Psi_j\right). \qquad (10)$$

Here $\hat{\mathbf{r}}_j$ represents the unit vector pointing outward from the origin located at the cube's center and Ω_S is the surface magnetization strength. H_S breaks $\mathcal{T}$ at the sample surface and a gap of size $\sim 2|\Omega_S|$ opens up in the spectrum of the surface states. Figure 3a shows the evolution of charge δQ accumulated near the intersection of the flux tube with the magnetized surface as a function of $\eta = \Phi/\Phi_0$. For small η we observe $\delta Q = \frac{1}{2}e\eta$, consistent with the fractional Hall conductivity $\sigma_{xy} = e^2/2h$ expected on the basis of Eq. (1). At $\eta = \frac{1}{2}$ a charge $e/2$ travels along the flux tube and combines with the negative charge that has built up on the opposite surface. For $\eta > \frac{1}{2}$ the charge δQ grows again at the rate controlled by σ_{xy} until it reaches $\delta Q = 0$ at $\eta = 1$. As already mentioned above, a Dirac string carrying a full flux quantum Φ_0 can be removed by a gauge transformation and the above evolution is thus consistent with the expectation that this weakly interacting system returns to the original configuration at the end of a full cycle.

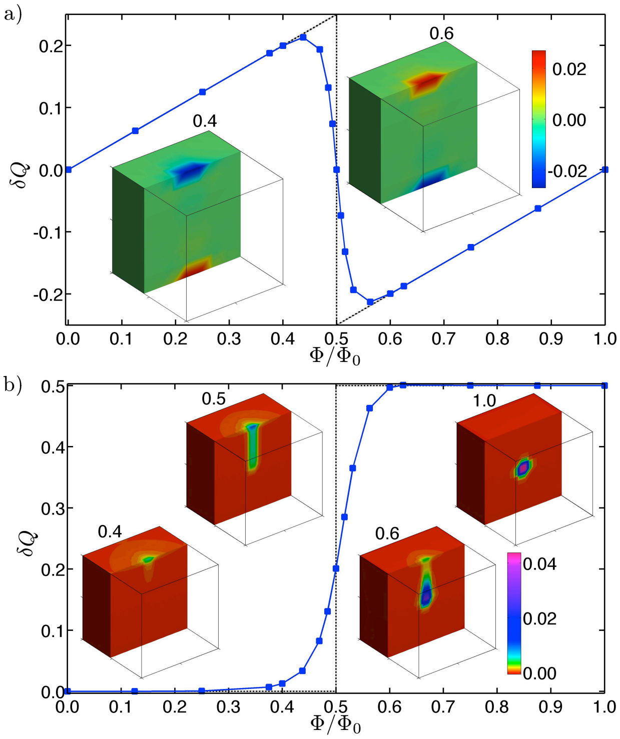

FIG. 3: (Color online) a) Charge δQ (in units of e) induced in the lower half of the sample by a flux tube carrying flux Φ. Insets show the charge density at indicated values of flux. b) Charge δQ in the sphere of radius r_0 centered at the monopole as a function of monopole strength. We have chosen $r_0 = 9.097$ so that the sphere is large enough to enclose the expected charge $e/2$ for the unit monopole projecting flux Φ_0. In both panels a cube-shaped sample with 20^3 lattice sites and parameters $t = 1$, $\epsilon = 4$ is used, $\Omega_S = 1, 0$ in a) and b) respectively. δQ is defined relative to the $\eta = 0$ situation.

Figure 3b displays a modified arrangement with the flux tube terminated by a magnetic monopole located at the center of the sample. This furnishes a realization of the Witten effect [17] in a STI [16]. As a function of increasing η, the charge first accumulates at the intersection of the flux tube and the surface. At $\eta = \frac{1}{2}$ a charge $e/2$ travels along the wormhole to the monopole, the corresponding charge density clearly visible in the inset to Fig. 3b. At $\eta = 1$ the flux tube becomes invisible but the $e/2$ charge remains bound to the monopole as expected on the basis of general arguments [16, 17].

We performed similar calculations for flux tubes of various shapes and in the presence of weak non-magnetic disorder. In all cases we found low-energy modes associated with the $\eta = \frac{1}{2}$ flux tube confirming the topological robustness of the wormhole effect.

We now address the possibility of experimental detection of the wormhole effect predicted in this Letter. In a real physical system it is not possible to confine magnetic flux to an area of size comparable to the crystal lattice spacing as would be necessary to probe the wormhole effect in its pure form. However, it should be possible to observe a closely related effect in a nanoscale hole fabricated in a STI crystal with a uniform magnetic field applied parallel to its axis, Fig. 1b. Sweeping the magnetic field strength will result in a periodic variation of the conductance along the hole with minima at $n\Phi_0$ and maxima at $(n + 1/2)\Phi_0$ as the excitation spectrum oscillates between insulating and metallic. Such variations should be observable experimentally if certain conditions are met. First, the hole radius R must be sufficiently large so that several oscillations can be observed in the available range of the laboratory field B. This gives $R \gtrsim (N\Phi_0/\pi B)^{1/2}$ for N oscillations. Second, R must be sufficiently small so that the maximum spectral gap Eq. (7) is large compared to k_BT, or otherwise the oscillations in the conductance will be washed out by thermal broadening. This gives $R \lesssim \hbar v/\sqrt{2}k_BT$. Taking typical values $B = 10$T, $N = 10$, $v = 5 \times 10^5$m/s and $T = 1$K yields 36 nm $\lesssim R \lesssim$ 450 nm. Thus, the experimental challenge would lie in fabricating a sub-micron size hole (or an array of holes) in a STI crystal or a thick film and measuring the conductance along the holes.

Oscillations with period Φ_0 have been observed in recent conductance measurements on Bi_2Se_3 single-crystal nanoribbons (cross sections $6 - 10 \times 10^{-15}$m^2, consistent with the above bounds on R) in longitudinal magnetic field [23]. In these, the same effect as discussed above should occur for the topologically protected states on the outer surfaces of the nanoribbon. However, the observed positions of minima and maxima were *opposite* to those predicted by our theory, suggesting that conductance in these experiments is dominated by some competing effect. The oscillations reported in Ref. [23] clearly deserve a detailed theoretical study.

The wormhole effect introduced here is fundamentally different from the gapless modes predicted to exist along the core of a crystal dislocation in topological insulators [18]. These latter modes depend solely on the *weak* invariants $(\nu_1\nu_2\nu_3)$ whereas the wormhole effect depends on the more robust *strong* invariant ν_0. In this sense the wormhole effect is inherently three-dimensional while the gapless modes associated with a dislocation are more closely related to the zero-modes in 2-dimensional topological (spin-Hall) insulators with solitonic defects [19, 20]. Mathematically, the wormhole effect is related to the protected one-dimensional modes predicted to exist along vortex lines in the order parameter characterizing a topological Mott insulator [21]. Unfortunately, no topological Mott insulators are known to exist at present, although according to Ref. 22 the pyrochlore compounds $A_2Ir_2O_7$ ($A =$ Pr,Eu) may exhibit this behavior.

The wormhole effect studied in this Letter represents a distinct *bulk* manifestation of the unusual electron properties in a strong topological insulator. Its existence resolves a conceptual dichotomy that arises when Laughlin's argument is applied to the magnetized STI surface and exemplifies a unique bulk-surface correspondence inherent to STIs. A closely related counterpart of the wormhole effect should be observable in artificially engineered nanostructures fabricated from available STIs.

Acknowledgment — The authors are indebted to J. Moore, I. Garate, and C. Weeks for stimulating discussion, and especially to B. Seradjeh for help in formulating the experimental proposal. Support for this work came from NSERC, CIfAR and The China Scholarship Council.

Note added — When this work was close to completion we became aware of a preprint [15] which has identified, in a different context, the gapless modes on a surface of a STI cylinder threaded by flux $\Phi_0/2$.

[1] L. Fu, C. L. Kane, and E. J. Mele, Phys. Rev. Lett. **98** 106803 (2007).
[2] J. E. Moore and L. Balents, Phys. Rev. B **75** 121306(R) (2007).
[3] L. Fu and C. L. Kane, Phys. Rev. B **76**, 045302 (2007).
[4] R. Roy, Phys. Rev. B **79**, 195322 (2009).
[5] H. Zhang, C.-X. Liu, X.-L. Qi, X. Dai, Z. Fang, and S.-C. Zhang, Nature Phys. **5**, 438 (2009).
[6] D. Hsieh *et al.*, Nature **452**, 970 (2008).
[7] Y. Xia *et al.*, Nature Phys. **5**, 398 (2009).
[8] Y.L. Chen *et al.*, Science **325**, 178 (2009).
[9] X.-L. Qi, T.L. Hughes, and S.-C. Zhang, Phys. Rev. B **78**, 195424 (2008).
[10] A.M. Essin, J.E. Moore, D. Vanderbilt, Phys. Rev. Lett. **102**, 146805 (2009).
[11] D.-H. Lee, Phys. Rev. Lett. **103**, 196804 (2009).
[12] X.-L. Qi, R. Li, J. Zang, S.-C. Zhang, Science **323**, 1184 (2009).
[13] R. B. Laughlin, Phys. Rev. B **23**, 5632 (1981).
[14] R. B. Laughlin, Phys. Rev. Lett. **50**, 1395 (1983).
[15] P. M. Ostrovsky, I. V. Gornyi, A. D. Mirlin, arXiv:0910.1338.
[16] G. Rosenberg and M. Franz, arXiv:1001.3179.
[17] E. Witten, Phys. Lett. B **86**, 283 (1979).
[18] Y. Ran, Y. Zhang, and A. Vishwanath, Nature Phys. **5**, 298 (2009).
[19] Y. Ran, A. Vishwanath, and D.-H. Lee, Phys. Rev. Lett. **101**, 086801 (2008).
[20] X.-L. Qi and S.-C. Zhang, Phys. Rev. Lett. **101**, 086802 (2008).
[21] Y. Zhang, Y. Ran, and A. Vishwanath, Phys. Rev. B **79**, 245331 (2009).
[22] D. A. Pesin and L. Balents, arXiv:0907.2962.
[23] H. Peng *et al.*, arXiv:0908.3314.